LAWRENCE
LIVERMORE
NATIONAL
LABORATORY

LLNL-TR-707403

Final report on Tasks 3 & 4 for CRADA between LLNL and Amgen Inc.

T. O'Hara, X. Zhang, C. Villongco, F. Lightstone, D. Richards

October 28, 2016

Disclaimer

This work performed under the auspices of the U.S. Department of Energy by Lawrence Livermore National Laboratory under Contract DE-AC52-07NA27344.

Atrial Model Development and Prototype Simulations

This is the Final Report for the Amgen Inc. and LLNL CRADA. Results and findings from Tasks 3 & 4 are described below. Previous tasks are briefly summarized.

Task 3: "Input parameters prepared for a Cardioid simulation."

Task 4: "Report including recommendations for additional scenario development and post-processing analytic strategy."

Executive Summary:

- Anatomical, image-based human atrial mesh was procured from UC San Diego. The mesh was transposed to be compatible with Cardioid.

- The Grandi et al. 2011 human atrial cellular action potential model, with ionic currents and calcium cycling representative of sinus rhythm and chronic atrial fibrillation was chosen. The model was implemented in Cardioid, validated, and optimized.

- The Grandi model was tested and benchmarked in a uniform tissue block. Conductivity parameters were determined. Spatial and temporal discretization was shown to be adequate.

- The full atrial model, complete with left and right chamber cell types for sinus rhythm and chronic atrial fibrillation, was paced under various conditions, and results were visualized and analyzed.

Introduction:

The goal of this CRADA was to develop essential tools needed to simulate human atrial electrophysiology in 3-dimensions using an anatomical image-based anatomy and physiologically detailed human cellular model. The atria were modeled as anisotropic, representing the preferentially longitudinal electrical coupling between myocytes. Across the entire anatomy, cellular electrophysiology was heterogeneous, with left and right atrial myocytes defined differently. Left and right cell types for the "control" case of sinus rhythm (SR) was compared with remodeled electrophysiology and calcium cycling characteristics of chronic atrial fibrillation (cAF). The effects of Isoproterenol (ISO), a beta-adrenergic agonist that represents the functional consequences of PKA phosphorylation of various ion channels and transporters, was also simulated in SR and cAF to represent atrial activity under physical or emotional stress.

The motivation for simulating human atria is that atrial arrhythmias afflict several million people in the United States alone, with debilitating consequences including an

elevated risk of stroke [1]. Furthermore, therapeutic strategies are limited, and often are unsuccessful [2]. Ablation of tissue can be effective to prevent AF, but patients often require additional follow-up ablations, a procedure that is extremely tedious, time consuming, and imprecise. This is not ideal given that ablation is destructive and invasive.

The computer model developed for this CRADA will serve as an additional tool to help understand, predict and prevent atrial arrhythmia. The model also serves as a test-kit for exploring ideas for new therapeutic strategies, and assessment of risk (c.f. review on the utility of atrial simulation [3]).

Convergence Test in Uniform, Anisotropic Tissue Slab:

With the Grandi human atrial action potential model [4] implemented and verified in Cardioid (Task 2), we proceeded to test model convergence using a protocol inspired by Niederer et al. [5]. Time to first activation was calculated at sites along a tissue slab of dimension 3x7x20 mm (see Figure 1, copied below from Niederer [5]). Fiber directions were uniform along the long axis of the slab, and conductivity was set to be ten-fold greater along the fiber axis than along orthogonal directions. A similar anisotropy ratio was used by others [6], and was based on local measurements of conduction [7], and histology [8]. Conductivity was scaled to result in wavefront propagation speeds that were similar to measurements from human atria (73±5 cm/s for control, sinus rhythm [9]).

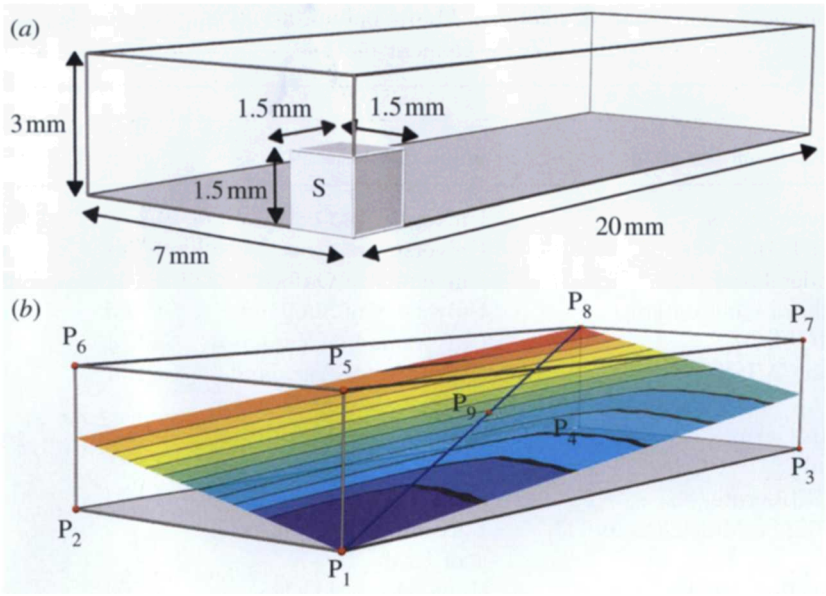

Figure 1. *Niederer tissue slab (copied from* [5]*). a) A box-shaped stimulus (S) delivered excitatory current to a corner of the slab (box side length of 1.5 mm^3, amplitude -35.71429 A/F, duration 2 ms). The slab was 3x7x20 mm, with fibers directed uniformly along the long, 20 mm axis. b) Activation time was recorded at corner locations P1 – P8 and at the slab center (P9). Conduction velocity was measured as the average speed of conduction from P1 to P8 (the ratio of path distance and difference in activation times). Colors show representative activation isochrones with the earliest activation in dark blue and the latest in red.*

We performed the Neiderer-based protocol using various combinations of spatial and temporal discretization. Spatial discretization was explored in the neighborhood of 0.13 mm, given that the atrial mesh that was prepared by colleagues Drs. Chris Villongco and Andrew McCulloch at UC San Diego had near-cellular resolution at 0.129247 mm (~0.13 mm, cubic elements). Temporal discretization was explored in the neighborhood of 0.01 ms. This choice was based on work for Task 2, in which we reported that the Grandi human atrial cell model was stably and rapidly integrated in single myocytes in Cardioid using a constant time step dt = 0.01 ms and forward Euler integration scheme (or the Rush-Larsen method [10] for stiff gates such as those governing the fast sodium current).

Results in Figure 2 shows that conduction velocity was relatively unaffected by space and time step variations in the neighborhood of 0.13 mm and 0.01 ms, respectively. Importantly, conduction velocity was <6% different between conditions to be used in simulations (dx = 0.13 mm, dt = 0.01 ms) and a more finely discretized case (dx = 0.10 mm, dt = 0.001 ms). Thus, we asserted that the atrial anatomy, provided by UCSD subcontract, was sufficiently resolved at dx = 0.13 mm to yield convergent simulation results, given a time step of size dt = 0.01 ms.

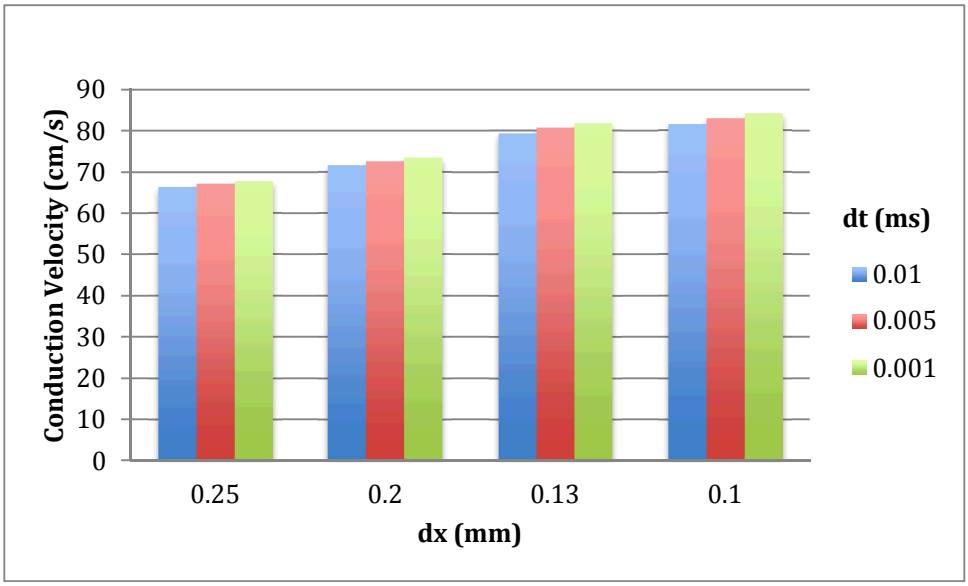

Figure 2. *Convergence of conduction velocity. For dt ≤ 0.01 ms (colored bars), and dx from 0.25 to 0.1 mm (left to right), conduction speed was relatively constant, and in an acceptable physiological range* [7,9].

Eigenvector to Tensor:

The atrial anatomy generated by UCSD colleagues was described using unit-scaled eigenvectors to indicate fiber, sheet, and sheet-normal conductivity directions. This eigenvector trio preserves the most general description of anisotropy, from which one can derive conductivity tensors or parameters relevant for simulating biomechanics. However, the Cardioid anatomy reader accepts conductivity tensors to describe

connectivity. We therefore specified diffusivity quantities, and followed the linear algebra shown in the Appendix, to make the conversion from eigenvector to tensor. The global identification numbers (gids) in the UCSD-generated anatomy files were also adjusted to make them compatible with Cardioid code (indexed from zero, not unity).

Coarsened Tetrahedral Mesh for Sensor Points and Visualization:

The atrial anatomy, at 0.13 mm spatial resolution, contains 31,476,981 records. For the sake of general-purpose visualization of simulation results, 31M voltage outputs are unnecessary and cumbersome. Therefore, similar to the visualization process for the ventricles in Cardioid, we specified a coarsened tetrahedral mesh that serves to designate a list of gids. These gids were used as "sensors" for transmembrane voltage or other model output to be saved to files for analysis and visualization. Tetrahedra were equilateral, and sensors were sampled evenly. The list of sensors for coarsening contains 273,532 entries (~1 mm resolution, ~10-fold coarsening). Both the sensors list (sensor.txt) and the coarsened equilateral tetrahedral mesh (coarse.vtk), illustrated below in Figure 3, are provided in Supplementary Materials.

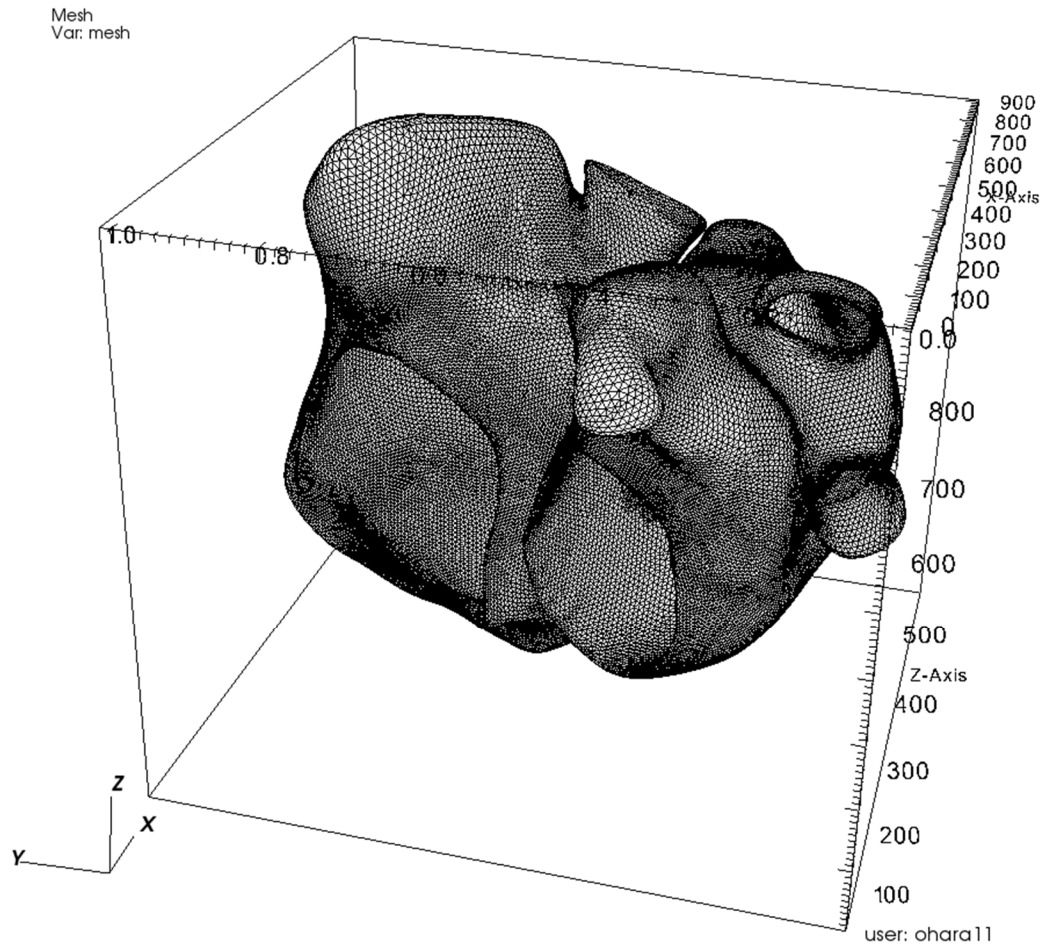

Figure 3. *Equilateral tetrahedral mesh for coarsened sensor designation and visualization. Spatial dimensions shown are by index, used to define gids (approximately 0 to 1000) for x, y, and z.*

A Voronoi coarsening algorithm within the Cardioid source code calculates the average voltage in the neighborhood of each sensor, along with the neighborhood size (in number of nodes, nvals), and saves them as delimited output at each sampled time step: gid, nvals, voltage.

Spatial Tagging of Left and Right Cell Types:

The Grandi human atrial model includes separate parameter sets for descriptions for right and left atrial action potentials. There are four total cell types: right and left for sinus rhythm (SR, control) and also right and left for chronic atrial fibrillation (cAF, see Task 2 report or Figure 7A from Grandi et al. [4]). Cardioid can establish region specific cell type in the anatomy file, where gid is associated with a flag for cell type.

Anatomy files for SR and for cAF with right and left atria designated, were created via the following steps. First, the coarse tetrahedral mesh was loaded into Paraview (Sandia Corporation, Kitware Inc.). Next, we divided the left and right atria by removing either the left atria (leaving only the right) or the right atria (leaving only the left). The left-only and right-only atria in VTK descriptions served as templates for the high-resolution mesh in anatomy files to map on. The mapping procedure was accomplished by looping over all gids in the anatomy files, and for each, we calculated the distance between each gid and nodes in VTK files. The shortest distance between the gid and left atria, as well as the shortest distance between the gid and right atria, were determined. If the gid was closer to the left atria, it was annotated as a left atria gid, (or the same for right). The total number of distances we needed to calculated was the product of the number of gids in the mesh (31,476,981) and the number of the nodes in VTK files (273,532), which is very large (~10 trillion calculations). To speed up the calculations, the square of distance was calculated instead of the distance itself so that the computationally expensive function, square root (sqrt), was avoided. Although the code was written in python and is single thread, we were able to pack many single thread jobs into a bundle job. In the end, a new anatomy template was created with placeholders for left and right (Figure 4). This labeled anatomy was converted from eigenvector to tensor format (see above and Appendix for details) with the additional step of replacing placeholders with flags to specify right and left for either SR or cAF.

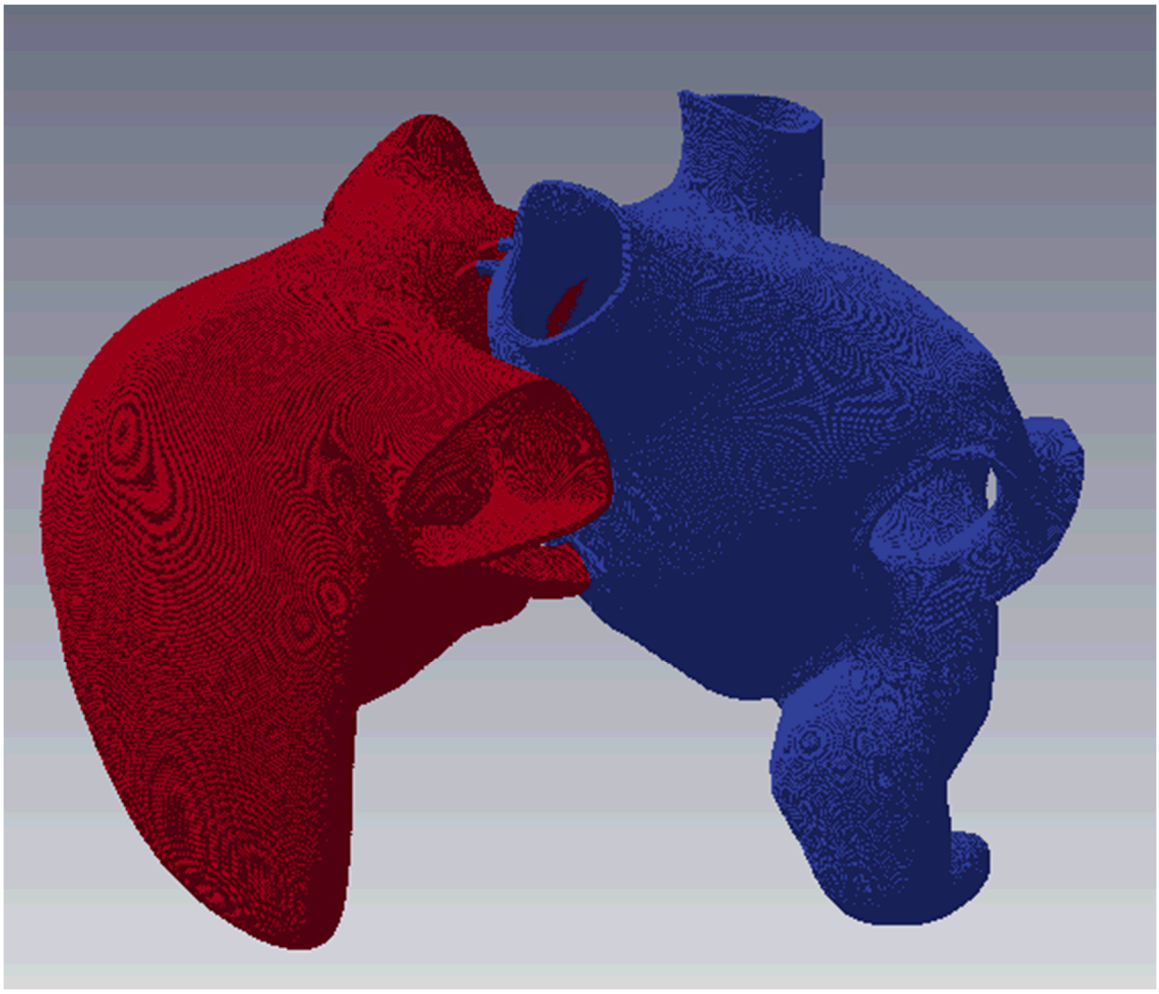

Figure 4. *Atrial anatomy showing right (red) and left (blue) atria tagged to specify regional cell type. This sidedness definition was used for both sinus rhythm and atrial fibrillation simulations.*

Sino-Atrial Nodal Pacing:

In order to represent physiological atrial pacing, we placed a stimulus "box" (30x30x30 elements, i.e., box side length of 3.9 mm, 60 A/F injected current for 1 ms) at the site of the sino-atrial node (SA node): i.e. at the nexus of the superior vena cava and the base of the right atrial appendage (Figure 5). The control SA nodal pacing rate was 1 Hz. In addition, we also tested pacing from the SA-node at 2 Hz, as well as the effect of adding isoproterenol (ISO) to represent physical or emotional stress.

These simulation results have been made into four movies, included in Supplementary Materials: 1) SR, 1 Hz SA-nodal pacing, basal conditions, 2) cAF, 1 Hz SA-nodal pacing, basal conditions, 3) SR, 2 Hz SA-nodal pacing, with ISO, and 4) cAF, 2 Hz SA-nodal pacing, with ISO. Movies show voltage color maps on the atrial surface as it changes with time. Three views of the atria are shown: anterior (large panel), posterior, and inferior. A line graph shows the voltage trace and the action potential near the SA nodal pacing site. Details of the movie layout are described in the Appendix. Action potential shape and duration depends on disease state and conditions.

Pulmonary Vein Triggers:

Atrial arrhythmia is often triggered in part by ectopic triggered activity from the pulmonary vein (PV) sleeves [11]. This has long been appreciated [12], and consequently, PVs are routinely electrically isolated from the atria using ablation techniques. In order to represent PV ectopy, we introduced a stimulus box on the left superior ostia (same dimensions, amplitude and duration as SA node stimulus see Figure 5 below). Wavefronts from PV origin were expected to appear as tachycardia/flutter arrhythmia. Alternatively, PV wavefronts could interact with physiological SA nodal activity, possibly leading to unidirectional block and reentry. Thus, the PV stimulus was introduced to provoke arrhythmia. PV stimulus cycle length and phase relative to SA nodal pacing was variable.

In cAF, PV-sleeve triggers at cycle lengths of 100, 150, 200, 250, and 300 ms were simulated. Triggers arriving in under 200 ms intervals resulted in stimuli delivered to PV cells that were already partially excited from the previous activation and were thus refractory. In all cases, PV wavefronts merged with SA nodal fronts and did not result in unidirectional block or reentry. Movies with results from these simulations are included in Supplementary Materials.

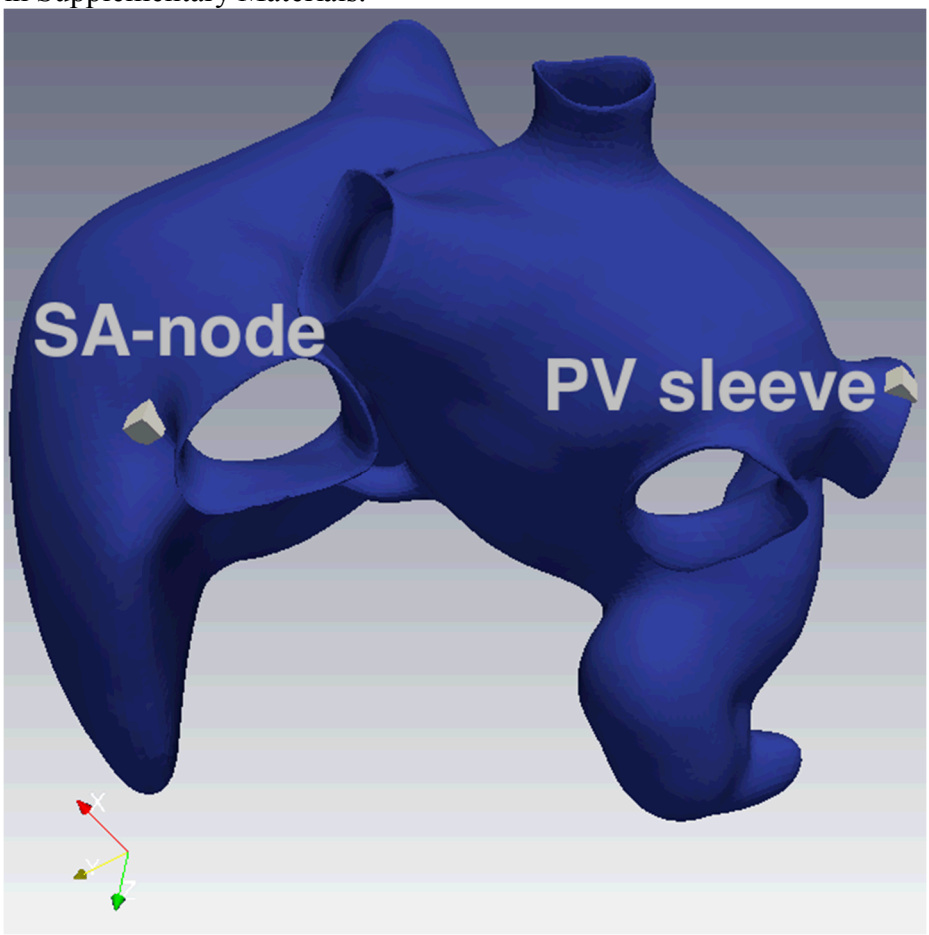

Figure 5. *A stimulus box was located at the sino-atrial node (SA-node) to simulate physiological pacing. The optional pulmonary vein sleeve stimulus box (PV sleeve) was included (or not) to simulate ectopic activity that regularly originates from this region and may be responsible for initiating flutter or fibrillation.*

Analysis, Discussion and Future Directions:

Simulations of essential atrial function in SR and for cAF were established and executed using Cardioid and LLNL high performance computers. Essential function was defined as SA nodal pacing under basal and stress conditions. We also simulated the effect of PV triggers and the interaction with basal pacing. None of the cases resulted in unidirectional block formation, or reentry, or naturally occurring ectopy such as could be caused by a prominent early or delayed afterdepolarization. We conclude that additional risk factors must be considered in order to elicit arrhythmia.

Application of drugs and channel block should alter these results, perhaps prolonging the action potential in some region(s) with coupling intervals that lead to unidirectional block and/or reentry, and/or formation of local afterdepolarizations that propagate out as ectopic foci. This multifactorial set of conditions can be part of future work. So too can heterogeneous presentation of fibrosis and scar, both expected to contribute to the arrhythmic substrate, as others have concluded [13].

Implementation of additional heterogeneous cell electrophysiological properties and cell types has been shown by others using islands of uniform cell type [14]. Ideally, regionality can be parameterized to create atria with a smoothly varying linear combinations of cellular properties, and not simply a mosaic of homogenous patches or islands. Evidence in support of such significantly and smoothly varying electrophysiological and ultrastructural properties has been shown in human experiments by Glukhov et al [15], and could be simulated in future work. In disease, regional properties can be affected by remodeling in a regionally dependent manner. This may lead to the formation of naturally occurring ectopy from some locations (i.e. PV), and if so, they can be explored to determine the underlying ionic mechanisms.

The Grandi cell model [16] can be augmented to represent more processes that are affected by disease or drugs. For example, we could include ion channel currents that are not in the original formulation, such as the small-conductance calcium-activated potassium current (SK current, or ISK). Another example is the ATP-sensitive potassium current, IKATP, which depends on and requires a description of cellular energy production and consumption (e.g. [17]). We could represent a cell model of paroxysmal atrial fibrillation type (pAF), adhering to the pAF remodeling changes outlined by others [18], to compare with already available SR and cAF types.

The effect of drugs of interest can be represented (e.g. dofetilide, ranolazine and amiodarone). These drugs primarily affect the cell by blocking ion channels. This could be represented by reducing the conductance of blocked channels and/or by replacing the original Hodgkin-Huxley current and gating formulations with Markov models for channel gating that include state-dependent drug block and detailed kinetics of drug binding and unbinding.

Simulations in Cardioid use a fine, near-cellular resolution. Future analysis and simulations could be designed to specifically exploit this feature and utilize it for investigating microstructural fibrosis and the consequence of detailed fibrosis and scar patterning.

In future work, it will be interesting to begin simulations by loading in heterogeneous initial conditions that correspond to regional cell types and implement a

pacing history that affects ionic balance and function. The atria are never at rest *in vivo*, and so a procedure for non-rest initiation should be considered in future work.

References:

1. Mozaffarian D, Benjamin EJ, Go AS, Arnett DK, Blaha MJ, Cushman M, et al. Heart Disease and Stroke Statistics—2016 Update [Internet]. Circulation. 2015. doi:10.1161/CIR.0000000000000350
2. Woods CE, Olgin J. Atrial fibrillation therapy now and in the future: Drugs, biologicals, and ablation. Circ Res. 2014;114: 1532–1546. doi:10.1161/CIRCRESAHA.114.302362
3. Trayanova NA. Mathematical Approaches to Understanding and Imaging Atrial Fibrillation: Significance for Mechanisms and Management. Circ Res. 2014;114: 1516–1531. doi:10.1161/CIRCRESAHA.114.302240
4. Grandi E, Pandit S V., Voigt N, Workman AJ, Dobrev D, Jalife J, et al. Human atrial action potential and Ca2+ model: sinus rhythm and chronic atrial fibrillation. Circ Res. 2011;109: 1055–66. doi:10.1161/CIRCRESAHA.111.253955
5. Niederer S a., Kerfoot E, Benson a. P, Bernabeu MO, Bernus O, Bradley C, et al. Verification of cardiac tissue electrophysiology simulators using an N-version benchmark. Philos Trans R Soc A Math Phys Eng Sci. 2011;369: 4331–4351. doi:10.1098/rsta.2011.0139
6. Zahid S, Whyte KN, Schwarz EL, Blake RC, Boyle PM, Chrispin J, et al. Feasibility of using patient-specific models and the "minimum cut" algorithm to predict optimal ablation targets for left atrial flutter. Hear Rhythm. Elsevier; 2016;13: 1687–1698. doi:10.1016/j.hrthm.2016.04.009
7. Hansson A, Holm M, Blomström P, Johansson R, Lührs C, Brandt J, et al. Right atrial free wall conduction velocity and degree of anisotropy in patients with stable sinus rhythm studied during open heart surgery. Eur Heart J. 1998;19: 293–300. doi:10.1053/euhj.1997.0742
8. Saffitz JE, Kanter HL, Green KG, Tolley TK, Beyer EC. Tissue-specific determinants of anisotropic conduction velocity in canine atrial and ventricular myocardium. Circ Res. 1994;74: 1065–1070. doi:10.1161/01.RES.74.6.1065
9. Konings KT, Kirchhof CJ, Smeets JR, Wellens HJ, Penn OC, Allessie MA. High-density mapping of electrically induced atrial fibrillation in humans. Circulation. 1994;89: 1665–1680. doi:10.1161/01.CIR.89.4.1665
10. Rush S, Larsen H. A practical algorithm for solving dynamic membrane equations. Biomed Eng IEEE Trans …. 1978;25: 389–392. Available: http://ieeexplore.ieee.org/xpls/abs_all.jsp?arnumber=4122859
11. Sánchez-Quintana D, López-Mínguez JR, Pizarro G, Murillo M, Cabrera JA. Triggers and anatomical substrates in the genesis and perpetuation of atrial fibrillation. Curr Cardiol Rev. 2012;8: 310–26. Available: http://www.pubmedcentral.nih.gov/articlerender.fcgi?artid=3492815&tool=pmcentrez&rendertype=abstract
12. Haïssaguerre M, Jaïs P, Shah DC, Takahashi A, Hocini M, Quiniou G, et al. Spontaneous Initiation of Atrial Fibrillation by Ectopic Beats Originating in the Pulmonary Veins. http://dx.doi.org.prxy4.ursus.maine.edu/101056/NEJM199809033391003. 2009; 659–666.
13. McDowell KS, Vadakkumpadan F, Blake R, Blauer J, Plank G, Macleod RS, et al.

Mechanistic inquiry into the role of tissue remodeling in fibrotic lesions in human atrial fibrillation. Biophys J. 2013;104: 2764–2773. doi:10.1016/j.bpj.2013.05.025
14. Adeniran I, MacIver DH, Garratt CJ, Ye J, Hancox JC, Zhang H. Effects of Persistent Atrial Fibrillation-Induced Electrical Remodeling on Atrial Electro-Mechanics – Insights from a 3D Model of the Human Atria. PLoS One. 2015;10: e0142397. doi:10.1371/journal.pone.0142397
15. Glukhov A V, Balycheva M, Sanchez-Alonso JL, Ilkan Z, Alvarez-Laviada A, Bhogal N, et al. Direct Evidence for Microdomain-Specific Localization and Remodeling of Functional L-Type Calcium Channels in Rat and Human Atrial Myocytes. Circulation. 2015;132: 2372–84. doi:10.1161/CIRCULATIONAHA.115.018131
16. Grandi E, Pandit S V., Voigt N, Workman AJ, Dobrev D, Jalife J, et al. Human Atrial Action Potential and Ca2+ Model: Sinus Rhythm and Chronic Atrial Fibrillation. Circ Res. 2011;109: 1055–1066. doi:10.1161/CIRCRESAHA.111.253955
17. Zhou L, Cortassa S, Wei AC, Aon MA, Winslow RL, O'Rourke B, et al. Modeling cardiac action potential shortening driven by oxidative stress-induced mitochondrial oscillations in guinea pig cardiomyocytes. Biophys J. Biophysical Society; 2009;97: 1843–1852. doi:10.1016/j.bpj.2009.07.029
18. Voigt N, Heijman J, Wang Q, Chiang DY, Li N, Karck M, et al. Cellular and Molecular Mechanisms of Atrial Arrhythmogenesis in Patients With Paroxysmal Atrial Fibrillation. Circulation. 2013;129: 145–56. doi:10.1161/CIRCULATIONAHA.113.006641
19. Durrer D, van Dam RT, Freud GE, Janse MJ, Meijler FL, Arzbaecher RC. Total excitation of the isolated human heart. Circulation. 1970;41: 899–912. doi:10.1161/01.CIR.41.6.899

Appendix:

Derivation of Conductivity Tensor for Fiber, Sheet, and Sheet-normal Eigenvectors:

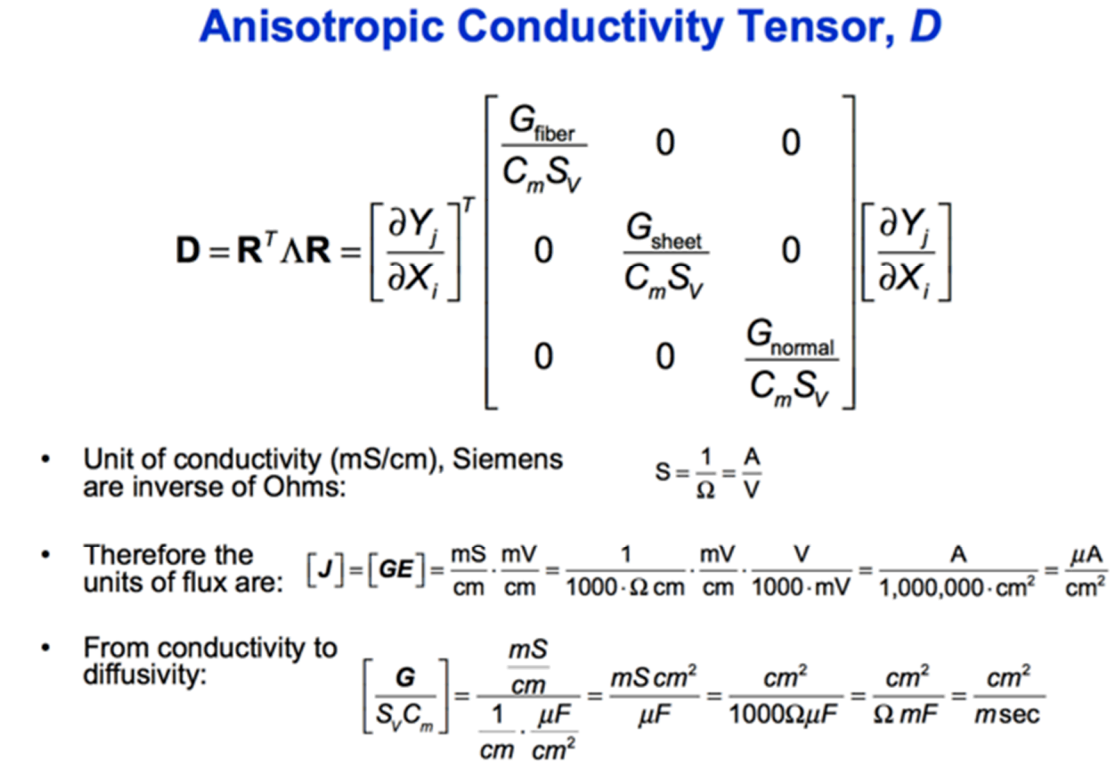

Figure A1. *Matrix mathematics for the conversation from eigenvector to tensor descriptions of fiber direction. Taken from Andrew McCulloch's UCSD lecture slides, available for free online (week 8, Feb 25th, http://cmrg.ucsd.edu/Courses/be276/Topics)*

In algebraic terms, for the trio of eigenvectors,

fiber: F=(f1, f2, f3)
sheet: S=(s1, s2, s3)
sheet-normal: N=(n1, n2, n3)

and given a lumped diffusivity parameter.

G=(Gf, Gs, Gn)
where Gf=10*Gf=10*Gn (i.e. diffusivity is 10-fold greater along the fiber direction)

then the tensor is …

sigma11 = Gf*f1*f1 + Gs*f2*f2 + Gn*f3*f3
sigma22 = Gf*s1*s1 + Gs*s2*s2 + Gn*s3*s3
sigma33 = Gf*n1*n1 + Gs*n2*n2 + Gn*n3*n3

sigma12 = Gf*f1*s1 + Gs*f2*s2 + Gn*f3*s3
sigma13 = Gf*f1*n1 + Gs*f2*n2 + Gn*f3*n3
sigma23 = Gf*s1*n1 + Gs*s2*n2 + Gn*s3*n3

The degree of diffusivity for defining the lumped parameter, G=(Gf, Gs, Gn), with components along fiber, sheet, and normal directions, is not a directly experimentally measurable quantity. The value can be indirectly inferred based on conduction speed, which is observable, and a rule for anisotropy of conduction (Gf=10*Gf=10*Gn, justified earlier).

The choice of Gf = 0.6 cm^2/ms (and Gs=Gn=0.06 cm^2/ms) resulted in full atrial activation from a sino-atrial nodal stimulus to the left atrial appendage within ~100 ms. This 100 ms target was based on invasive measurements in human atria (see activation maps in Figure 5 of Durrer et al. [19]).

Description of Movie Files and Layout:

In all movies included in Supplementary Materials, membrane voltage is shown by colors ranging from purple (resting voltage, -90 mV) to yellow (activated, +50 mV). The large panel on the left shows the anterior view. Below the anterior view is a trace of the voltage (action potential) at the SA nodal region near the pacing site. On the right are posterior (above) and inferior (below) views of the atria. Simulation time can be tracked by following the voltage trace and the vertical marker indicating the time being shown in ms.